

Parabolic Hall effect due to Co-Propagating Surface Modes

M. Breitzkreuz*

*Dahlem Center for Complex Quantum Systems and Fachbereich Physik,
Freie Universität Berlin, 14195 Berlin, Germany*

(Dated: November 2019)

Real-space separations of counter-moving states to opposite surfaces or edges are associated with different types of Hall effects, such as the quantum-, spin-, or the anomalous Hall effect. Some systems provide the possibility to separate a fraction of counter-movers in a completely different fashion: Surface states propagating all in the same direction, balanced by counter-moving bulk states, realized, e.g., in Weyl metals with intrinsically or extrinsically broken inversion and time-reversal symmetries. In this work we show that these co-propagating surface modes are associated with a novel Hall effect — a parabolic potential profile in the direction perpendicular to and in its magnitude linear in the applied field. While in 2D systems the parabolic potential profile is measurable directly, in 3D the resulting voltage between bulk and surface is measurable in the geometry of a hollow cylinder. Moreover, the parabolic Hall effect leads to characteristic signatures in the longitudinal conductivity.

Introduction—The condensed-matter realization of Weyl fermions [1–9] has attracted very much interest in the past years, due in large part to the realization of chiral Landau levels, moving parallel or antiparallel to the magnetic field, depending on the Weyl-fermion chirality [10]. In a crystal, the two chiralities appear pairwise, separated in momentum space, which complicates an identification of Weyl-specific transport phenomena such as the chiral magnetic effect [11–14].

Tentatively it is more promising when chiral states are separated not (or not only) in momentum but in real space — a situation well known from the separation of counter-movers to opposite surfaces in topological insulators [15]. Here the favorable situation associated with the real-space separation is the clear signature in form of a quantum (spin) Hall effect [16, 17]. A noteworthy pendant in the field of Weyl metals is the anomalous Hall effect (AHE) [18, 19] — a voltage drop in the direction perpendicular to both, the direction of the current flow and the intrinsic magnetization, in the absence of an external magnetic field [20–22]. The mechanism of the AHE in Weyl metals can indeed be understood in terms of chiral surface states — a pairwise connection of Weyl Fermi surfaces of opposite chirality by two Fermi arcs [23], localized at opposite surfaces and moving in opposite directions, which intuitively explains the AHE as the contribution of Fermi arcs in case of a potential difference between the surfaces [8, 24], see Fig. 1. Remarkably, the presence of a finite density of diffusive bulk states does not obscure the chiral-surface-states driven AHE.

In this work we focus on a different and much less explored separation of counter-movers in real space: forward-movers homogeneously distributed in the bulk and back-movers localized at the surface. This can be realized in 2D systems [25] (edge states have been called “antichiral” in this case), including transition-metal dichalcogenide monolayers [25], and exciton-polariton systems [26], and in 3D Weyl metals [27, 28]. Comparing

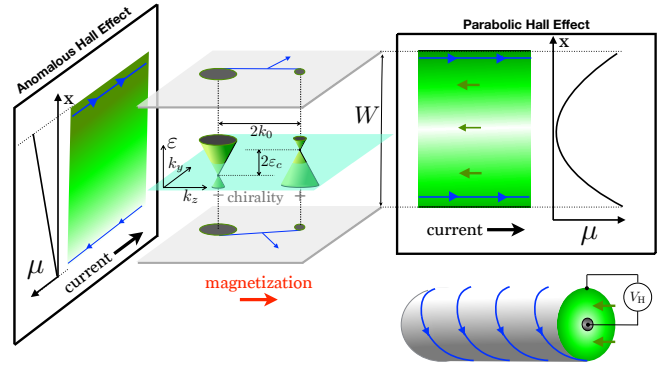


FIG. 1. Weyl-metal slab with two Weyl cones separated in energy and in momentum, connected by Fermi arcs at the surfaces, illustrated in a mixed momentum/real space. Anomalous Hall effect — a linear drop of the chemical potential μ between the surfaces — occurs if current is led in the plane of counter-propagating surface modes. The parabolic Hall effect occurs when current is led in the plane of co-propagating surface modes, leading to a quadratic spatial dependence of μ , measurable in the geometry of a hollow cylinder between the inner and outer surfaces.

to the well-studied case of counter-propagating surface modes the question arises, whether co-propagating surface modes can also be associated with a characteristic Hall effect.

We show that the answer is positive — co-propagating surface modes give rise to a novel Hall response, characterized by a *quadratic* spatial dependence of the chemical potential μ , transverse to the applied field. The general mechanism can be understood as follows. In the bulk, the current density of chiral charge carriers (the fraction of bulk charges compensating the current of co-propagating surface states) changes proportional to the local chemical potential, $\delta j_c \propto \delta \mu$. Together with the coexisting diffusive bulk charges flowing according to $j_n \propto \nabla \mu$, the total current must be divergence free in the steady state,

hence $\nabla^2\mu \propto -\hat{j}_c \cdot \nabla\mu$, where \hat{j}_c is the direction of the chiral bulk current. If now a homogeneous electric field $\mathbf{E} = -\nabla\mu$ is applied along \hat{j}_c , the chemical potential assumes a quadratic spatial dependence in the direction perpendicular to the applied field. This is what we call the parabolic Hall effect (PHE). Note that this effect is still linear in the driving field and thus distinct from effects called “non-linear Hall effect” [29].

In the following we explore the effect in detail. We focus on a minimal 3D model of a Weyl metal, Fig. 1, which, while allowing direct conclusion on the simpler case of 2D, requires additional calculations to show how the resulting Hall voltage can be measured in 3D systems.

Model—Measuring energy in units of $\hbar v$, where v is the Fermi velocity, and length in units of the lattice constant, the Hamiltonian we consider reads

$$H = -\sigma_x i \partial_x + k_y \sigma_y + m(k_z) \sigma_z + \varepsilon_c \eta(k_z), \quad (1)$$

where σ_i are spin Pauli matrices, $m(k_z) = (k_z^2 - k_0^2)/2k_0$, and $\eta(k_z) = \tanh(2k_z/k_0)$, featuring two Weyl nodes with chirality \pm at momentum $k_{x,y} = 0$, $k_z = \pm k_0$ and energy $\varepsilon \approx \pm \varepsilon_c$.

We focus on the case of two well-separated Weyl cones with vanishing corrections to the linear dispersion and a constant velocity v at the Fermi level ε_F , hence $\varepsilon_c, |\varepsilon_F| \ll k_0$. The explicit form of $m(k_z)$ and $\eta(k_z)$ is unimportant as long as these requirements are fulfilled.

Considering a slab of width W the quantum numbers are $\boldsymbol{\kappa} = (q, k_y, k_z)$, where q is the solution of

$$\frac{m(k_z)}{q} \tan(Wq) + 1 = 0 \quad (2)$$

coming from the boundary condition of the slab [30]. Throughout this work we assume $W \gg 1$, in which case the solution for q can be divided into three groups, (i) the group of bulk states, given by the quasi continuous set $q = (n + 0.5)\pi/W$, $n = 0, 1, 2, \dots$, (ii) surface states

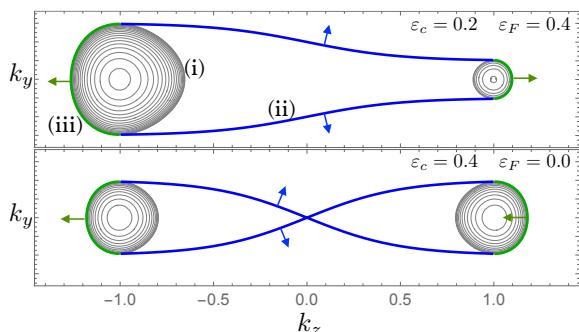


FIG. 2. Fermi-level states for the Weyl metal of width $W = 100$, $k_0 = 1$, and two different combinations of ε_F and ε_c . The gray, blue, and green states correspond to (i) normal bulk state, (ii) surface states, and (iii) chiral bulk states, respectively. Velocity directions are indicated by arrows.

with the imaginary (and hence exponentially decaying) solution $q = i m(k_z)$ for $m(k_z) < 0$, and (iii) chiral bulk states with the solution $q = 0$ for $m(k_z) > 0$. The dispersion reads

$$\varepsilon_{\boldsymbol{\kappa}} = \varepsilon_c \eta(k_z) \pm \sqrt{q^2 + k_y^2 + [m(k_z)]^2} \quad (3)$$

and the equi-energy contours are illustrated in Fig. 2. Note that surface states (ii) and chiral bulk states (iii) merge at $m(k_z) = 0$ building a single closed contour.

Since the x dependence of the wavefunctions is given by $\exp(iq x)$, the finite penetration depth of surface states is $1/\text{Im} q$. The velocity of a wave packet at state $\boldsymbol{\kappa}$ can thus be written as $\mathbf{v}_{\boldsymbol{\kappa}} = \text{Re}[(\partial_q, \partial_{k_y}, \partial_{k_z})\varepsilon_{\boldsymbol{\kappa}}]$ and the free spectral function in the center-of-mass coordinate x and the $W \gg 1$ limit reads

$$A(\boldsymbol{\kappa}, x, \omega) = 2\pi\delta(\omega - \varepsilon_{\boldsymbol{\kappa}})\rho(\boldsymbol{\kappa}, x), \quad (4)$$

$$\rho(\boldsymbol{\kappa}, x) = \begin{cases} 1 & \text{Im} q = 0 \\ 2W m(k_z) e^{\pm 2m(k_z)(x \mp W/2)} & \text{Im} q \neq 0 \end{cases} \quad (5)$$

where $\text{Im} q = 0$ and $\text{Im} q \neq 0$ distinguishes bulk and surface states, and \pm corresponds to surface states at $x = \pm W/2$. Despite the divergence of penetration at $m(k_z) = 0$, the surface-state spectral weight averaged over all states at the surface is strongly localized, the characteristic length scale being $1/k_0 \sim 1$. Since all other length scales will be considered to be much larger, we approximate the $\text{Im} q \neq 0$ case in (S3) as $\rho(\boldsymbol{\kappa}, x) \approx W\delta(x \mp W/2)$ in the following.

The density of bulk states at the Fermi level of the cone \pm and the total bulk density $n_n = \sum_{\pm} n_{n\pm}$, read, respectively,

$$n_{n\pm} = \frac{(\varepsilon_F \mp \varepsilon_c)^2}{\pi v h}, \quad n_n = 2 \frac{\varepsilon_F^2 + \varepsilon_c^2}{\pi v h}. \quad (6)$$

We also define the density of chiral bulk states and the 2D density of surface states of a single surface,

$$n_{c\pm} = \frac{|\varepsilon_F \mp \varepsilon_c|}{2v h W}, \quad n_s = \frac{k_0}{\pi v h}, \quad (7)$$

respectively. In accord with $W \gg 1$, we assume that n_n is much larger than $n_{c\pm}$ and n_s/W .

Parabolic Hall effect—To explore the transport behavior in linear response, we aim to find a solution for a state-dependent deviation of the chemical potential from the Fermi energy, $\mu(\boldsymbol{\kappa})$, with an arbitrary spatial profile along the x direction, given the boundary condition of a homogeneous force field applied in the z direction, $\partial_z \mu(\boldsymbol{\kappa}) = E$. Furthermore we assume elastic scattering from a weak disorder potential. To focus on qualitative features, we take the scattering amplitudes different only between Fermi-level states of the different types

$i \in [n+, c+, s+, n-, c-, s-]$. Using the Quantum Boltzmann formalism [31] and employing the standard semiclassical approximation scheme, see Supplemental Material for details [32], we obtain

$$\nabla \cdot (\mathbf{j}_{n\pm} + \mathbf{j}_{c\pm}) = \pm \gamma_{n-n+}(\mu_{n-} - \mu_{n+}) + \gamma_{sn\pm}s(x)(\mu_s - \mu_{n\pm}), \quad (8a)$$

$$s(x) \nabla \cdot \mathbf{j}_{s\pm} = s(x) [\gamma_{sn+}(\mu_{n+} - \mu_{s\pm}) + \gamma_{sn-}(\mu_{n-} - \mu_{s\pm})], \quad (8b)$$

$$\mathbf{j}_{n\pm} = -n_{n\pm}D \nabla \mu_{n\pm}, \quad (8c)$$

where $\gamma_{ij} = \Gamma_{ij}n_in_j$ and Γ_{ij} is the scattering rate, $\mu_i = \langle \mu(\boldsymbol{\kappa}) \rangle_i$ is the local chemical potential averaged over the Fermi-level states i , $\mathbf{j}_i = n_i(\mathbf{v}_{\boldsymbol{\kappa}}\mu(\boldsymbol{\kappa}))_i$ is the non-equilibrium current-density contribution of the states i , D is the bulk diffusion constant, and $s(x) = \sum_{\pm} \delta(x \pm W/2)$.

To linear order in E and using translation invariance in the y direction, the divergence of the chiral-bulk and the surface particle currents simplify to

$$\nabla \cdot \mathbf{j}_{c\pm} = \pm \frac{\varepsilon_F \mp \varepsilon_c}{\pi h W} E, \quad \nabla \cdot \mathbf{j}_{s\pm} = \frac{\varepsilon_c}{\pi h} E. \quad (9)$$

We rewrite Eqs. (8) by considering the differential Eqs. (8a) away from the boundary ($s(x) = 0$), together with (8c) and (9),

$$\pm \frac{\varepsilon_F \mp \varepsilon_c}{\pi h W} E - n_{n\pm}D \partial_x^2 \mu_{n\pm} = \pm \gamma_{n+n-}(\mu_{n-} - \mu_{n+}). \quad (10)$$

This is supplemented with boundary conditions, given by integration of (8) over an infinitesimal distance at both boundaries and assuming vanishing current through the boundary,

$$j_{n+}^x(\pm W/2) = \mp \gamma_{sn+}(\mu_{s\pm} - \mu_{n+}(\pm W/2)), \quad (11a)$$

$$j_{n-}^x(\pm W/2) = \mp \gamma_{sn-}(\mu_{s\pm} - \mu_{n-}(\pm W/2)), \quad (11b)$$

$$\begin{aligned} \frac{\varepsilon_c}{\pi h} E &= \gamma_{sn+}(\mu_{n+}(\pm W/2) - \mu_{s\pm}) \\ &+ \gamma_{sn-}(\mu_{n-}(\pm W/2) - \mu_{s\pm}). \end{aligned} \quad (11c)$$

Assuming that an external contact would couple to all bulk states with equal probability it would probe the averaged chemical potential

$$\mu_n = \frac{n_{n+}\mu_{n+} + n_{n-}\mu_{n-}}{n_n}, \quad (12)$$

for which Eqs. (10) and (11) readily provide the solution

$$\mu_n = -\frac{n_s v}{n_n D} \frac{\varepsilon_c}{k_0} \frac{x^2}{W} E + z E. \quad (13)$$

Sticking to the interpretation that E is an applied field in the z direction, the response lies in the first term in (13), which exhibits the PHE — a quadratic spatial dependence on the transverse coordinate x and a linear dependence of the magnitude of the applied field E . The

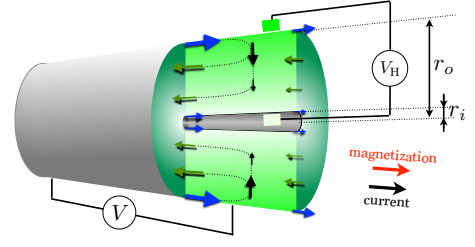


FIG. 3. Weyl metal in the geometry of a hollow cylinder with a small inner radius. When current is led along the cylinder and the magnetization, the PHE voltage is induced between the inner and the outer surface. Arrows indicate local current flows of chiral bulk (green), surface (blue), and diffusive bulk (black) particles.

roles of applied and induced fields are of course interchangeable so that a finite magnitude of the transverse potential would induce a finite longitudinal field E and with that a longitudinal current (which will be calculated below).

Measuring the Hall voltage—In contrast to the ordinary Hall effect where the potential varies linearly and is fully characterized by a voltage between opposite surfaces, the PHE voltage occurs between one surface and the bulk and varies quadratically with the distance. While in a 2D system the parabolic voltage profile can be measured directly, in a 3D system a contact inside the sample necessarily introduces an inner surface so that the actual geometry for such a measurement is (in its most simple realization) that of a hollow cylinder, see Fig. 3, with an inner radius r_i and an outer radius r_o . A straightforward modification of the above formalism [32] [essentially consisting in the replacements $W \rightarrow r_o - r_i$, $x \rightarrow r$, $\partial_x j_n^x \rightarrow (\partial_r + 1/r)j_n^r$] leads to the solution

$$\mu_n(r) = -\frac{n_s v}{n_n D} \frac{\varepsilon_c}{k_0} \left(\frac{r^2/2}{r_o - r_i} - \frac{r_o r_i}{r_o - r_i} \ln \frac{r}{r_i} \right) E + z E. \quad (14)$$

We quantify the voltage between the inner and the outer surfaces via the resulting Hall angle $\theta_{\text{PHE}} \equiv [\mu_n(r_o) - \mu_n(r_i)]/(r_o - r_i)E$. In the limit $r_o \gg r_i$ we obtain

$$\theta_{\text{PHE}} = -\frac{n_s v}{n_n D} \frac{\varepsilon_c}{2k_0}. \quad (15)$$

Note that the first factor, $n_s v/n_n D \equiv \theta$, is the Hall angle of the AHE [19, 24], which is thus related to θ_{PHE} by the ratio of energy- vs. momentum separation of the Weyl nodes (energy in units of $\hbar v$).

Conductivity—We first note that general symmetry considerations [33, 34] fix the form of the infinite-system conductivity tensor of our system to

$$\sigma = \begin{pmatrix} \sigma^{xx} & \sigma^{xy} & 0 \\ -\sigma^{xy} & \sigma^{xx} & 0 \\ 0 & 0 & \sigma^{zz} \end{pmatrix}, \quad (16)$$

which follows from rotation symmetry around z and symmetry with respect to time reversal combined with C_2 rotation around an x - y -plane axis, corresponding to the Laue group $\infty 2'$ [33]. As discussed above, the model exhibits AHE in the x - y plane, with a Hall angle $\sigma^{xy}/\sigma^{xx} = \theta$, related to the intrinsic magnetization in the z direction. The PHE is instead found in the plane parallel to z but it evidently does not manifest itself in a finite σ^{xz} or σ^{yz} , which is in agreement with our result that the potential difference in the x direction between outer surfaces vanishes.

In the following we show that the PHE still manifests itself in the infinite-system conductivity — it gives rise to an anomalous term in σ^{zz} , which is size-dependent but finite in the infinite-system limit. The current contribution of normal bulk states in response to the field E is obtained from (8c) as $j_n^z = -n_n D E$. This would be the only contribution to σ^{zz} that one would obtain for an infinite system based on the Drude formula; we denote it as $\sigma_0^{zz} \equiv j_n^z/E$. The additional contributions of chiral bulk states and surface states, neglecting corrections of order $1/W$, can be written as $j_{c\pm}^z = \pm(\varepsilon_F \mp \varepsilon_c) \mu_{n\pm}/\pi\hbar W$ and $j_{s\pm}^z = \delta(x \mp W/2) \mu_{s\pm} \varepsilon_c/\pi\hbar$, respectively. Inserting μ_i as solutions of (10) and (11), the full conductivity is given by $\sigma^{zz} = (j_n^z + \bar{j}_c^z + \bar{j}_s^z)/E$, where the bar denotes averaging over x . In terms of σ_0^{zz} we obtain

$$\frac{\sigma^{zz}}{\sigma_0^{zz}} = 1 + \frac{4}{3} \theta_{\text{PHE}}^2 \left(1 + \frac{6l_{ns}}{W\theta} \right) \left(1 + \frac{\varepsilon_F^2}{\varepsilon_c^2} \xi \right), \quad (17)$$

$$\xi = \frac{\frac{2l_c}{W} - \frac{\left(\frac{2l_c}{W}\right)^2}{\frac{l_{ns}}{\theta l_c} + \coth \frac{W}{2l_c}}}{\frac{W}{6l_c} + \frac{l_{ns}}{\theta l_c}} = \begin{cases} 0 & l_c \ll W \\ 1 & l_c \gg W, l_{ns}/\theta, \end{cases} \quad (18)$$

where $l_{ns} = v/\Gamma_{sn} n_n$ is the relaxation length of surface states and $l_c = \sqrt{D/\Gamma_{n+n} n_n}$ is the internode relaxation length [35]. In the infinite-system limit we obtain $\sigma^{zz} = (1 + 4\theta_{\text{PHE}}^2/3)\sigma_0^{zz}$, demonstrating a remarkable deviation from the Drude behavior. We expect that the same correction can be derived based purely on the bulk Hamiltonian, e.g., using Kubo formalism. We leave this for future work, noting that similarly exchangeable derivations from an infinite- and a finite-system perspective have been demonstrated for the AHE in [19] and [24].

The finite-size correction in the first brackets is similar to the finite-size correction of the AHE in [24] and is due to the vanishing dissipation of surface states if their scattering length becomes large compared to the width W . The second brackets correspond to a finite-size correction which occurs if the system is not electron-hole compensated ($\varepsilon_F \neq 0$), in which case the applied field induces an occupation disbalance between the Weyl nodes leading to a prolonged relaxation time. The resistivity decrease saturates even if $l_c \rightarrow \infty$ because internode relaxation also happens indirectly via surface states.

Discussion—Our calculations have shown that co-propagating surface modes and the related counter-propagating bulk states (which we here call chiral) give rise to a parabolic transverse potential profile. We made the realistic assumption that the density of coexisting normal bulk states (spatially not separated counter-movers) is finite and hence $\sim W$ times larger than the number of surface states, where W is the width in units of the lattice constant. Nevertheless, the spatial separation of surface and chiral bulk states by $\sim W$ compensates this so that the PHE survives the limit $W \rightarrow \infty$. Besides the Hall voltage, we have identified an anomalous term in the longitudinal conductivity, which can be interpreted as the precursor of the anomalously large conductance in the quantum regime of localized normal bulk states [25, 36].

We exemplified the parabolic Hall effect on a model for a Weyl metal with intrinsically broken inversion and time-reversal symmetries, which shows a homogeneous chiral charge density in the bulk [37]. Several ways have been proposed to induce (or change) the chiral charge density in Weyl metals externally. For example, internode charge pumping via parallel electric and magnetic fields can effectively shift the energies of the Weyl nodes as

$$\varepsilon_c \rightarrow \varepsilon_c + \frac{e^2}{\hbar^2} \frac{\tau}{n_n} EB, \quad (19)$$

where τ is the internode relaxation time, which is assumed to be much larger than intranode relaxation [11]. Another interesting possibility to induce and control the PHE is the application of a strain-induced pseudomagnetic field [28, 36, 38], which allows to change the density of chiral states even without an electric field and independent of the internode relaxation.

Furthermore, the derived unconventional dependence of the conductivity on the system size and the scattering amplitudes as a consequence of the PHE is an interesting starting and reference point for investigations of the conductivity with regard to temperature dependence in case of phonon-mediated scattering [39], or the scaling behaviour with the system size [40]. It is worth noting that in a time-reversal invariant Weyl metal, the mechanism of a reduced and size-dependent resistivity due to a doubling of the AHE [24], also applies to the PHE. The PHE voltage would vanish but the associated suppression of the resistivity would remain when the coupling between the time-reversed states is sufficiently weak. The suppression would set in when the width W becomes comparable to the characteristic scattering length quantifying the coupling of time-reversed states.

Acknowledgments. The author would like to thank Piet W. Brouwer, Tobias Meng, and Rodrigo G. Pereira for valuable discussions. This research was supported by the Grant No. 18688556 of the Deutsche Forschungsgemeinschaft (DFG, German Research Foundation).

-
- * breitkr@physik.fu-berlin.de
- [1] S.-Y. Xu, N. Alidoust, I. Belopolski, Z. Yuan, G. Bian, T.-R. Chang, H. Zheng, V. N. Strocov, D. S. Sanchez, G. Chang, C. Zhang, D. Mou, Y. Wu, L. Huang, C.-C. Lee, S.-M. Huang, B. Wang, A. Bansil, H.-T. Jeng, T. Neupert, A. Kaminski, H. Lin, S. Jia, and M. Zahid Hasan, *Science* **349**, 613 (2015).
 - [2] S.-Y. Xu, N. Alidoust, I. Belopolski, Z. Yuan, G. Bian, T.-R. Chang, H. Zheng, V. N. Strocov, D. S. Sanchez, G. Chang, C. Zhang, D. Mou, Y. Wu, L. Huang, C.-C. Lee, S.-M. Huang, B. Wang, A. Bansil, H.-T. Jeng, T. Neupert, A. Kaminski, H. Lin, S. Jia, and M. Zahid Hasan, *Nat. Phys.* **11**, 748 (2015).
 - [3] B. Q. Lv, H. M. Weng, B. B. Fu, X. P. Wang, H. Miao, J. Ma, P. Richard, X. C. Huang, L. X. Zhao, G. F. Chen, Z. Fang, X. Dai, T. Qian, and H. Ding, *Phys. Rev. X* **5**, 031013 (2015).
 - [4] S. Borisenko, Q. Gibson, D. Evtushinsky, V. Zabolotnyy, B. Büchner, and R. J. Cava, *Phys. Rev. Lett.* **113**, 027603 (2014).
 - [5] M. Neupane, S.-Y. Xu, R. Sankar, N. Alidoust, G. Bian, C. Liu, I. Belopolski, T.-R. Chang, H.-T. Jeng, H. Lin, A. Bansil, F. Chou, and M. Z. Hasan, *Nat. Commun.* **5**, 3786 (2014).
 - [6] Z. K. Liu, B. Zhou, Y. Zhang, Z. J. Wang, H. M. Weng, D. Prabhakaran, S. K. Mo, Z. X. Shen, Z. Fang, X. Dai, Z. Hussain, and Y. L. Chen, *Science* **343**, 864 (2014).
 - [7] J. Xiong, S. K. Kushwaha, T. Liang, J. W. Krizan, M. Hirschberger, W. Wang, R. J. Cava, and N. P. Ong, *Science* **350**, 413 (2015).
 - [8] N. P. Armitage, E. J. Mele, and A. Vishwanath, *Rev. Mod. Phys.* **90**, 015001 (2018).
 - [9] B. Yan and C. Felser, *Annu. Rev. Condens. Matter Phys.* **8**, 337 (2017).
 - [10] H. B. Nielsen and M. Ninomiya, *Phys. Lett. B* **130(6)**, 389 (1983).
 - [11] A. A. Burkov, *Annu. Rev. Condens. Matter Phys.* **9**, 359 (2018).
 - [12] A. A. Burkov, *Phys. Rev. B* **96**, 041110(R) (2017).
 - [13] S. Nandy, G. Sharma, A. Taraphder, and S. Tewari, *Phys. Rev. Lett* **119**, 176804 (2017).
 - [14] R. D. dos Reis, M. O. Ajeesh, N. Kumar, F. Arnold, C. Shekhar, M. Naumann, M. Schmidt, M. Nicklas, and E. Hassinger, *New J. Phys.* **18**, 085006 (2016).
 - [15] X. L. Qi and S. C. Zhang, *Rev. Mod. Phys.* **83**, 1057 (2011).
 - [16] K. von Klitzing, *Rev. Mod. Phys.* **58**, 519 (1986).
 - [17] M. König, S. Wiedmann, C. Brüne, A. Roth, H. Buhmann, L. W. Molenkamp, X.-L. Qi, and S.-C. Zhang, *Science* **318**, 766 (2007).
 - [18] A. A. Burkov and L. Balents, *Phys. Rev. Lett* **107**, 127205 (2011).
 - [19] A. A. Burkov, *Phys. Rev. Lett* **113**, 187202 (2014).
 - [20] T. Suzuki, R. Chisnell, A. Devarakonda, Y.-T. Liu, W. Feng, D. Xiao, J. W. Lynn, and J. G. Checkelsky, *Nat. Phys.* **12**, 1119 (2016).
 - [21] E. Liu, Y. Sun, L. Müchler, A. Sun, L. Jiao, J. Kroder, V. Süß, H. Borrmann, W. Wang, W. Schnelle, S. Wirth, S. T. B. Goennenwein, and C. Felser, *Nat. Phys.* **14**, 1125 (2018).
 - [22] P. Li, J. Koo, W. Ning, J. Li, L. Miao, L. Min, Y. Zhu, Y. Wang, N. Alem, C.-X. Liu, Z. Mao, and B. Yan, arXiv:1910.10378.
 - [23] L. Balents, *Physics (College Park, Md.)* **4**, 36 (2011).
 - [24] M. Breitzkreuz and P. W. Brouwer, *Phys. Rev. Lett* **123**, 066804 (2019).
 - [25] E. Colomé and M. Franz, *Phys. Rev. Lett.* **120**, 086603 (2018).
 - [26] S. Mandal, R. Ge, and T. C. Liew, *Phys. Rev. B* **99**, 115423 (2019).
 - [27] P. Baireuther, J. A. Hutasoit, J. Tworzydło, and C. W. J. Beenakker, *New J. Phys* **18**, 045009 (2016).
 - [28] D. I. Pikulin, A. Chen, and M. Franz, *Phys. Rev. X* **6**, 041021 (2016).
 - [29] I. Sodemann and L. Fu, *Phys. Rev. Lett.* **115**, 216806 (2015).
 - [30] N. Bovenzi, M. Breitzkreuz, T. E. O'Brien, J. Tworzydło, and C. W. J. Beenakker, *New J. Phys.* **20**, 023023 (2018).
 - [31] G. D. Mahan, *Many-Particle Physics* (Kluwer Academic, New York, 2000).
 - [32] See Supplemental Material for details of the derivation and solution of transport equations for the slab and the hollow-cylinder geometry.
 - [33] W. H. Kleiner, *Phys. Rev.* **142**, 318 (1966).
 - [34] M. Seemann, D. Ködderitzsch, S. Wimmer, and H. Ebert, *Phys. Rev. B* **92**, 155138 (2015).
 - [35] S. A. Parameswaran, T. Grover, D. A. Abanin, D. A. Pesin, and A. Vishwanath, *Phys. Rev. X* **4**, 031035 (2014).
 - [36] J. Behrends, R. Ilan, and J. H. Bardarson, *Phys. Rev. Res.* **1**, 032028 (2019).
 - [37] More generally, a non-linear potential is produced by chiral states acting as particle sources or drains when a driving field E_{\parallel} is aligned with their motion, $\nabla^2 \mu = E_{\parallel} / \lambda$, where the characteristic length λ given by the relative densities and mobilities of the chiral and diffusive particles might be spatially inhomogeneous.
 - [38] A. G. Grushin, J. W. F. Venderbos, A. Vishwanath, and R. Ilan, *Phys. Rev. X* **6**, 041046 (2016).
 - [39] R. G. Pereira, F. Bucccheri, A. De Martino, and R. Egger, *Phys. Rev. B* **100**, 035106 (2019).
 - [40] C. Zhang, Z. Ni, J. Zhang, X. Yuan, Y. Liu, Y. Zou, Z. Liao, Y. Du, A. Narayan, H. Zhang, T. Gu, X. Zhu, L. Pi, S. Sanvito, X. Han, J. Zou, Y. Shi, X. Wan, S. Y. Savrasov, and F. Xiu, *Nat. Mater.* **18**, 482 (2019).

SUPPLEMENTAL MATERIAL

Quantum Boltzmann formalism

To explore the transport behavior in linear response, but at the same time allowing non-linear dependencies on the spatial coordinate, we use the Quantum Boltzmann Transport formalism [31] allowing an arbitrary spatial variation of the Wigner distribution function at state $\boldsymbol{\kappa}$, $f(\boldsymbol{\kappa}, \mathbf{r}, \omega)$, where \mathbf{r} denotes the three-dimensional center-of-mass position. In this inhomogeneous case, an external field, inducing the steady non-equilibrium state, can be incorporated via non-equilibrium boundary conditions on the spatial variation of the distribution, hence no explicit external field will be needed. Assuming impurity scattering in first Born approximation (T matrix given by impurity-potential matrix elements $V_{\boldsymbol{\kappa}\boldsymbol{\kappa}'}$) and assuming that the associated renormalization of the dispersion relation is already incorporated in $\varepsilon_{\boldsymbol{\kappa}}$, the kinetic equation reads

$$\mathbf{v}_{\boldsymbol{\kappa}} \cdot \nabla f(\boldsymbol{\kappa}, \mathbf{r}, \omega) = A(\boldsymbol{\kappa}, \mathbf{r}, \omega) \int \frac{d^3 \boldsymbol{\kappa}'}{(2\pi)^3} |V_{\boldsymbol{\kappa}\boldsymbol{\kappa}'}|^2 f(\boldsymbol{\kappa}', \mathbf{r}, \omega) - f(\boldsymbol{\kappa}, \mathbf{r}, \omega) \int \frac{d^3 \boldsymbol{\kappa}'}{(2\pi)^3} |V_{\boldsymbol{\kappa}\boldsymbol{\kappa}'}|^2 A(\boldsymbol{\kappa}', \mathbf{r}, \omega). \quad (\text{S1})$$

Following the standard route, from the Wigner distribution function $f(\boldsymbol{\kappa}, \mathbf{r}, \omega)$ we factor out the spectral density $A(\boldsymbol{\kappa}, \mathbf{r}, \omega)$ such that $f(\boldsymbol{\kappa}, \mathbf{r}, \omega) = f(\boldsymbol{\kappa}, \mathbf{r})A(\boldsymbol{\kappa}, \mathbf{r}, \omega)$, defining the non-equilibrium occupation function $f(\boldsymbol{\kappa}, \mathbf{r})$. Assuming weak scattering, we employ the quasiparticle approximation and use the free-particle expression for the spectral function (from the main text),

$$A(\boldsymbol{\kappa}, \mathbf{r}, \omega) = \delta(\omega - \varepsilon_{\boldsymbol{\kappa}}) \rho(\boldsymbol{\kappa}, x), \quad (\text{S2})$$

$$\rho(\boldsymbol{\kappa}, x) = \begin{cases} 1 & \text{Im } q = 0 \\ 2Wm(k_z) e^{\pm 2m(k_z)(x \mp W/2)} & \text{Im } q \neq 0 \end{cases} \quad (\text{S3})$$

Inserting into (S1) and integrating over ω , we obtain the Boltzmann equation

$$\mathbf{v}_{\boldsymbol{\kappa}} \cdot \nabla f(\boldsymbol{\kappa}, \mathbf{r}) = \sum_{\boldsymbol{\kappa}'} \Gamma_{\boldsymbol{\kappa}\boldsymbol{\kappa}'} [f(\boldsymbol{\kappa}', \mathbf{r}) - f(\boldsymbol{\kappa}, \mathbf{r})], \quad (\text{S4})$$

where we divided both sides by $\rho(\boldsymbol{\kappa}, x)$ (keeping in mind that Eq. (S4) becomes trivial if $\rho(\boldsymbol{\kappa}, x) = 0$, i.e., for surface states away from the boundary). In the Boltzmann Equation we defined

$$\sum_{\boldsymbol{\kappa}'} \Gamma_{\boldsymbol{\kappa}\boldsymbol{\kappa}'} \dots = \int \frac{d^3 \boldsymbol{\kappa}'}{(2\pi)^3} |V_{\boldsymbol{\kappa}\boldsymbol{\kappa}'}|^2 \delta(\varepsilon_{\boldsymbol{\kappa}} - \varepsilon_{\boldsymbol{\kappa}'}) \rho(\boldsymbol{\kappa}', x) \dots \quad (\text{S5})$$

To focus more deeply on qualitative features, we assume that the scattering amplitudes are different only between states of the different types, so that $\Gamma_{\boldsymbol{\kappa}\boldsymbol{\kappa}'} \rightarrow \Gamma_{ij}$, where $i, j \in [n+, c+, s+, n-, c-, s-]$. In this case, the integral over states naturally splits into integrals over the different particle types at the Fermi level,

$$\begin{aligned} \sum_{\boldsymbol{\kappa}'} &= \sum_{\boldsymbol{\kappa}'}^{n\pm} + \sum_{\boldsymbol{\kappa}'}^{c\pm} + s(x) \sum_{\boldsymbol{\kappa}'}^s, \\ \sum_{\boldsymbol{\kappa}'}^{n\pm} &= \int^{n\pm} \frac{d^2 \boldsymbol{\kappa}'}{4\pi^2 \hbar v}, \quad \sum_{\boldsymbol{\kappa}'}^{c\pm} = \frac{1}{W} \int^{c\pm} \frac{d\boldsymbol{\kappa}'}{2\pi \hbar v}, \quad \sum_{\boldsymbol{\kappa}'}^s = \int^{s\pm} \frac{d\boldsymbol{\kappa}'}{2\pi \hbar v}, \end{aligned} \quad (\text{S6})$$

where $s(x) = \sum_{\pm} \delta(x \pm W/2)$. Since the Boltzmann equation (S4) is non-trivial only for the non-equilibrium part of the occupation, the usual ansatz $f(\boldsymbol{\kappa}, \mathbf{r}) = n_F(\varepsilon_{\boldsymbol{\kappa}}) + n'_F(\varepsilon_{\boldsymbol{\kappa}}) \mu(\boldsymbol{\kappa}, \mathbf{r})$, where $n_F(\varepsilon_{\boldsymbol{\kappa}})$ is the equilibrium occupation function, replaces $f(\boldsymbol{\kappa}, \mathbf{r}) \rightarrow \mu(\boldsymbol{\kappa}, \mathbf{r})$ in (S4). We define the non-equilibrium chemical potential and the particle-current density of each particle type i , respectively, as

$$\mu_i = \langle \mu(\boldsymbol{\kappa}) \rangle_i = \sum_{\boldsymbol{\kappa}}^i \mu(\boldsymbol{\kappa}, \mathbf{r}) / n_i, \quad \mathbf{j}_{i\pm} = n_i \langle \mathbf{v}_{\boldsymbol{\kappa}} \mu(\boldsymbol{\kappa}, \mathbf{r}) \rangle_i = \sum_{\boldsymbol{\kappa}}^i \mathbf{v}_{\boldsymbol{\kappa}} \mu(\boldsymbol{\kappa}, \mathbf{r}), \quad (\text{S7})$$

where $n_i = \sum_{\boldsymbol{\kappa}}^i$ is the density of states of the particle type i . Defining the diffusion constant of bulk particles as $D = v^2/3 \sum_{\boldsymbol{\kappa}'} \Gamma_{n\pm \boldsymbol{\kappa}'}$ and summing the Boltzmann equation (S4) over $n\pm$ after multiplying with $\mathbf{v}_{\boldsymbol{\kappa}}$ and assuming the Weyl Fermi surfaces to be spherical, we obtain

$$\mathbf{j}_{n\pm} = -n_{\pm} D \nabla \mu_{n\pm}. \quad (\text{S8})$$

Summing the Boltzmann equation (S4) over each particle type gives

$$\nabla \cdot \mathbf{j}_{n\pm} = \pm (\gamma_{c\mp n\pm} + \gamma_{n-n+})(\mu_{n-} - \mu_{n+}) + \gamma_{sn\pm}s(x)(\mu_s - \mu_{n\pm}), \quad (\text{S9a})$$

$$\nabla \cdot \mathbf{j}_{c\pm} = \pm \gamma_{n\mp c\pm}(\mu_{n-} - \mu_{n+}) + \gamma_{sc\pm}s(x)(\mu_s - \mu_{c\pm}), \quad (\text{S9b})$$

$$s(x)\nabla \cdot \mathbf{j}_{s\pm} = s(x)[\gamma_{sn+}(\mu_{n+} - \mu_{s\pm}) + \gamma_{sn-}(\mu_{n-} - \mu_{s\pm}) + \gamma_{sc+}(\mu_{c+} - \mu_{s\pm}) + \gamma_{sc-}(\mu_{c-} - \mu_{s\pm})], \quad (\text{S9c})$$

where $\gamma_{ij} = \Gamma_{ij}n_in_j$ and we assumed that intracone scattering is much larger than intercone and bulk-surface scattering so that $\mu_{n\pm} - \mu_{c\pm} \approx 0$ away from the boundary. Taking into account that the number of normal bulk states n_{\pm} strongly dominates since $W \gg 1$ the equations simplify to Eqs. (11) in the main text.

Solving the transport equations

We now solve for the case of a homogeneous force field applied in the z direction in form of a potential gradient $\partial_z \mu = E$. To linear order in E and using translation invariance in the y direction, the divergence of the chiral and the surface particle currents simplify to

$$\nabla \cdot \mathbf{j}_{c\pm} = \bar{n}v_{c\pm}E, \quad \nabla \cdot \mathbf{j}_{s\pm} = \bar{n}v_s^z E, \quad (\text{S10})$$

where the density-of-states weighted integral over the velocity at the Fermi level reads

$$\bar{n}v_{c\pm} = \pm \frac{\varepsilon_F \mp \varepsilon_c}{\pi h W}, \quad \bar{n}v_s^z = \frac{\varepsilon_c}{\pi h} = \frac{\varepsilon_c}{k_0} n_s v. \quad (\text{S11})$$

A solution for the non-equilibrium potential profile in the x direction is found by first solving for the non-equilibrium potential for the bulk. Away from the boundary ($s(x) = 0$) we obtain from (S9), (S8), and (S10)

$$\bar{n}v_{c\pm}E - n_{n\pm}D\partial_x^2 \mu_{n\pm} = \pm \frac{n_+n_-}{n_n} \frac{D}{l_c^2} (\mu_{n-} - \mu_{n+}), \quad (\text{S12})$$

where we used $\gamma_{c-n+} + \gamma_{n-n+} + \gamma_{n-c+} \approx n_+n_- \Gamma_{n+n-}$ since $n_{c\pm} \ll n_{\pm}$ and defined the chiral relaxation length $l_c \equiv \sqrt{D/\Gamma_{n+n-n}}$. Boundary conditions for $\mu_{n\pm}$ are given by integration of (S9) over an infinitesimal distance at both boundaries and assuming vanishing current through the boundary,

$$j_{n+}^x(\pm W/2) = \mp \gamma_{sn+}(\mu_{s\pm} - \mu_{n+}(\pm W/2)), \quad (\text{S13a})$$

$$j_{n-}^x(\pm W/2) = \mp \gamma_{sn-}(\mu_{s\pm} - \mu_{n-}(\pm W/2)), \quad (\text{S13b})$$

$$E\bar{n}v_s^z = \gamma_{sn+}(\mu_{n+}(\pm W/2) - \mu_{s\pm}) + \gamma_{sn-}(\mu_{n-}(\pm W/2) - \mu_{s\pm}). \quad (\text{S13c})$$

We now introduce the bulk chemical potential μ_n , which is the local chemical potential averaged over all bulk states, and the chiral chemical potential μ_a ,

$$\mu_{n/a} = \frac{n_+ \mu_{n+} \pm n_- \mu_{n-}}{n_n} \Leftrightarrow \mu_{n\pm} = n_n \frac{\mu_n \pm \mu_a}{2n_{\pm}}. \quad (\text{S14})$$

In terms of μ_n and μ_a , Eqs. (S12) and the boundary conditions (S13) partially decouple into

$$\partial_x^2 \mu_n = -2\theta \frac{\varepsilon_c}{k_0} \frac{E}{W} \quad (\text{S15a})$$

$$\partial \mu_n \big|_{x=\pm W/2} = \mp \theta \frac{\varepsilon_c}{k_0} \frac{E}{W} \quad (\text{S15b})$$

$$\partial_x^2 \mu_a = \frac{1}{l_c^2} [\mu_a - \gamma \mu_n] + 2\theta \frac{\varepsilon_F}{k_0} \frac{E}{W}, \quad (\text{S15c})$$

$$\partial \mu_a \big|_{x=\pm W/2} = \mp \left[\theta \frac{\varepsilon_c}{k_0} \gamma \left(1 + \frac{\theta W}{4l_{ns}} \right) E + \frac{\theta}{l_{ns}} \mu_a \big|_{x=\pm W/2} \right], \quad (\text{S15d})$$

where $\gamma = (n_+ - n_-)/n_n$, $l_{ns} = v/\Gamma_{sn}n_n$ is the scattering length of surface states, and

$$\theta = \frac{n_s v}{n_n D} = \frac{v}{2D} \frac{k_0}{\varepsilon_c^2 + \varepsilon_F^2} \quad (\text{S16})$$

is the Hall angle of the AHE associated with the system of two Weyl nodes [18, 24].

The solution of (S15) together with the solution for μ_s from (S13c) read

$$\mu_n = -\theta \frac{\varepsilon_c}{k_0} \frac{x^2}{W} E + z E, \quad (\text{S17a})$$

$$\mu_a = -\frac{\theta}{k_0} W E \left[2 \left(\frac{l_c}{W} \right)^2 \left(\varepsilon_F + \varepsilon_c \gamma \right) \left(1 - \frac{\cosh \frac{x}{l_c}}{\frac{l_{ns}}{\theta l_c} \sinh \frac{W}{2l_c} + \cosh \frac{W}{2l_c}} \right) + \varepsilon_c \gamma \frac{x^2}{W^2} \right], \quad (\text{S17b})$$

$$\mu_{s\pm} = \mu_n|_{x=W/2} - \frac{\bar{n}v_s^z}{n_s v} l_{ns} E = -\frac{\varepsilon_c}{k_0} \theta \left(\frac{1}{4} + \frac{l_{ns}}{\theta W} \right) W E + z E. \quad (\text{S17c})$$

Hollow-cylinder geometry

We now calculate the potential μ_n in the geometry of a hollow cylinder. The derivation of the Boltzmann equation (S4) and summation over states leading to Eqs. (S9) is unmodified. For the calculation of μ_n it is sufficient to consider Eqs. (S8), (S9), and (S10), summed over \pm and the sum of n and c states, which then gives

$$\mathbf{j}_n = -n_n D \nabla \mu_n, \quad (\text{S18a})$$

$$\nabla \cdot (\mathbf{j}_n + \mathbf{j}_c) = -s(r) \nabla \cdot \mathbf{j}_s, \quad (\text{S18b})$$

$$\nabla \cdot \mathbf{j}_c = -2 \frac{\varepsilon_c}{k_0} \frac{n_s v}{r_o - r_i} E, \quad (\text{S18c})$$

$$\nabla \cdot \mathbf{j}_s = \frac{\varepsilon_c}{k_0} n_s v E, \quad (\text{S18d})$$

where we used (S10), $n_n \gg n_c$, the cancellation of the total equilibrium current,

$$\pi(r_o^2 - r_i^2) \sum_{\pm} \bar{n} v_{c\pm} + 2\pi(r_o + r_i) \bar{n} v_s^z = 0, \quad (\text{S19})$$

and the not altered result for the 2D density-of-states weighted integral over velocity of surface states (S11).

In cylinder coordinates the divergence $\nabla \cdot \mathbf{j}_n$ becomes $(\partial_r + 1/r) j_n^r$, leading to the differential equation

$$(\partial_r + 1/r) \partial_r \mu_n = -2\theta \frac{\varepsilon_c}{k_0} \frac{E}{r_o - r_i}. \quad (\text{S20})$$

The solution satisfying the boundary conditions given in (S18) reads

$$\mu_n = -\frac{n_s v}{n_n D} \frac{\varepsilon_c}{k_0} \left(\frac{r^2/2}{r_o - r_i} - \frac{r_o r_i}{r_o - r_i} \ln \frac{r}{r_i} \right) E + z E. \quad (\text{S21})$$

Defining the Hall angle for the PHE as $\theta_{\text{PHE}} \equiv [\mu_n(r_o) - \mu_n(r_i)] / (r_o - r_i) E$ in the limit $r_o \gg r_i$, we obtain

$$\theta_{\text{PHE}} = -\frac{n_s v}{n_n D} \frac{\varepsilon_c}{2k_0}. \quad (\text{S22})$$

Current density and conductivity

To obtain the longitudinal resistivity, we calculate the current densities in the z direction. From (S8) we obtain

$$j_n^z = -n_n D E. \quad (\text{S23})$$

The non-equilibrium current contribution of chiral bulk particles and surface states is given by

$$\begin{aligned} j_{s/c}^z(x) &= \frac{1}{W} \int \frac{dk_y dk_z d\omega}{(2\pi)^2} A(\boldsymbol{\kappa}, \mathbf{r}, \omega) n'_F(\varepsilon_{\boldsymbol{\kappa}}) \mu(\boldsymbol{\kappa}, \mathbf{r}) v_{\boldsymbol{\kappa}}^z \\ \Rightarrow j_s^z(x) &= \delta(x \pm W/2) \bar{n} v_s^z \mu_{s\pm} \end{aligned} \quad (\text{S24})$$

$$\Rightarrow j_c^z(x) = \sum_{\pm} \bar{n} v_{c\pm}^z \mu_{n\pm}, \quad (\text{S25})$$

where we used that the non-equilibrium part of the occupation function reads $n'_F(\varepsilon_{\boldsymbol{\kappa}}) \mu(\boldsymbol{\kappa}, \mathbf{r})$ (the equilibrium parts cancel each other as discussed in the main text) and neglected the variation of $\mu(\boldsymbol{\kappa}, \mathbf{r})$ with $\boldsymbol{\kappa}$ which would give a correction of order $1/W$. Now using Eq. (S14) and the solutions (S17) we obtain

$$\frac{j_c^z(x)}{j_n^z} = -\theta^2 \frac{\varepsilon_c^2}{k_0^2} \left[2 \left(\frac{x}{W} \right)^2 + \left(\frac{2l_c}{W} \right)^2 \frac{\varepsilon_F^2}{\varepsilon_c^2} \left(\frac{\cosh \frac{x}{l_c}}{\frac{l_{ns}}{\theta l_c} \sinh \frac{W}{2l_c} + \cosh \frac{W}{2l_c}} - 1 \right) \right], \quad (\text{S26})$$

$$\frac{j_s^z(x)}{j_n^z} = \theta^2 \frac{\varepsilon_c^2}{k_0^2} \left(\frac{1}{4} + \frac{l_{ns}}{\theta W} \right) W \sum_{\pm} \delta(x \pm W/2). \quad (\text{S27})$$

The resistivity is given by

$$\sigma^{zz} = \frac{\bar{j}_c^z + \bar{j}_s^z + j_n^z}{E}, \quad \bar{j}_i^z = \frac{1}{W} \int dx j_i^z(x). \quad (\text{S28})$$

In the absence of the PHE, i.e., if the potential would be homogeneous in the x direction, the contributions of surface and chiral bulk states would cancel each other (up to the neglected correction of order $1/W$). In this case, the current would be carried mainly via the normal bulk states and the resistivity would be given by $\sigma_0^{zz} = j_n^z/E = -n_n D$, which is also what one would obtain from the Drude formula for the conductivity of the infinite system. Now taking into account the effect of the PHE, the full conductivity in terms of σ_0^{zz} becomes

$$\frac{\sigma^{zz}}{\sigma_0^{zz}} = 1 + \frac{4}{3} \theta_{\text{PHE}}^2 \left(1 + \frac{6l_{ns}}{W\theta} \right) \left(1 + \frac{\varepsilon_F^2}{\varepsilon_c^2} \xi \right), \quad (\text{S29})$$

$$\xi = \frac{\frac{2l_c}{W} - \frac{\left(\frac{2l_c}{W}\right)^2}{\frac{l_{ns}}{\theta l_c} + \coth \frac{W}{2l_c}}}{\frac{W}{6l_c} + \frac{l_{ns}}{\theta l_c}} = \begin{cases} 0 & l_c \ll W \\ 1 & l_c \gg W, l_{ns}/\theta. \end{cases} \quad (\text{S30})$$